Automated Detection and Tracking of Individual and Clustered Cell Surface Low Density Lipoprotein Receptor Molecules

Richik N. Ghosh and Watt W. Webb
School of Applied and Engineering Physics, Cornell University, Ithaca, New York 14853 USA

ABSTRACT We have developed a technique to detect, recognize, and track each individual low density lipoprotein receptor (LDL-R) molecule and small receptor clusters on the surface of human skin fibroblasts. Molecular recognition and high precision (30 nm) simultaneous automatic tracking of all of the individual receptors in the cell surface population utilize quantitative time-lapse low light level digital video fluorescence microscopy analyzed by purpose-designed algorithms executed on an image processing work station. The LDL-Rs are labeled with the biologically active, fluorescent LDL derivative dil-LDL. Individual LDL-Rs and unresolved small clusters are identified by measuring the fluorescence power radiated by the sub-resolution fluorescent spots in the image; identification of single particles is ascertained by four independent techniques. An automated tracking routine was developed to track simultaneously, and without user intervention, a multitude of fluorescent particles through a sequence of hundreds of time-lapse image frames. The limitations on tracking precision were found to depend on the signal-to-noise ratio of the tracked particle image and mechanical drift of the microscope system. We describe the methods involved in (i) time-lapse acquisition of the low-light level images, (ii) simultaneous automated tracking of the fluorescent diffraction limited punctate images, (iii) localizing particles with high precision and limitations, and (iv) detecting and identifying single and clustered LDL-Rs. These methods are generally applicable and provide a powerful tool to visualize and measure dynamics and interactions of individual integral membrane proteins on living cell surfaces.

INTRODUCTION

Background

Lateral motion of integral membrane proteins plays an important part in many biological phenomena (Axelrod, 1983; McCloskey, 1984), and studies of protein mobility in the plane of the plasma membrane have been carried out for many receptors and cell types (Cherry, 1979; McCloskey, 1984; Webb et al., 1982). Most of these investigations have employed the technique of fluorescence photobleaching recovery (FPR), which yields ensemble averaged diffusion coefficients and mobile fractions of the protein species studied (Axelrod et al., 1976; Jacobson et al., 1982; Webb et al., 1982). FPR measurements have shown that the mobility of most proteins on cell membranes is so constrained that their diffusion coefficients are reduced by several orders of magnitude below their theoretical fluid dynamic values in a fluid lipid membrane (Saffman, 1976; Saffman and Delbrück, 1975). Some fraction of most molecular species appear immobile in FPR experiments (Axelrod, 1983; McCloskey, 1984). Nonetheless, lipids diffuse essentially as expected from the theoretical fluid dynamics prediction of Saffman and Delbrück (Saffman, 1976; Saffman and Delbrück, 1975). This suggests the existence of restraints impeding the free diffusion of proteins in cell membranes.

Constraints on membrane proteins might introduce correlations that would cause the statistical physics of their motion to deviate from free Brownian diffusion as well as to slow the random walk. Ideally, different types of protein motion should be revealed by FPR (Axelrod et al., 1976; Thomas and Webb, 1990), but due to the noisiness of actual data, all motion is necessarily assumed to be free Brownian diffusion modified only by an immobile fraction (Thomas and Webb, 1990). Because conventional FPR gives ensemble-averaged diffusion coefficients, the behavior of individual particles is masked. Active motion of proteins and other deviations from Brownian motion are inaccessible with FPR, although correlated concerted motion or flow may be recognizable by characteristic recovery kinetics (Axelrod et al., 1976; Thomas and Webb, 1990).

Repeated spot FPR experiments on the same system yield a wide range of diffusion coefficients whose spread far exceeds the deviation expected from measurement uncertainty. This wide range of diffusion coefficients has been attributed to the heterogeneity of individual molecular motions on cell membranes (Thomas and Webb, 1990). The microenvironment of certain regions of the cell membrane may cause proteins to move in a different manner from proteins in other areas (Yechiel and Edidin, 1987). Nevertheless, FPR cannot effectively reveal different types of motion occurring simultaneously on the cell because the signal that is collected simultaneously samples the mobility of many molecules in the surroundings of a photobleached spot (or interference pattern), about one micron in diameter; nor is conventional

Received for publication 25 October 1993 and in final form 22 February 1994.

Address reprint requests to Watt W. Webb, School of Applied Physics, Clark Hall, Cornell University, Ithaca, NY 14853-2501. Tel.: 607-255-3331; Fax: 607-255-7658.

Dr. Ghosh's current address: Pathology Department, College of Physicians and Surgeons, Columbia University, New York, NY 10032. Tel: 212-305-4091.

0006-3495/94/05/1301/18 $2.00

FPR a feasible tool for studying sparsely distributed receptors, because it requires a high density of labels to generate a sufficient number of photons for proper photon statistics.

To avoid these limitations, we developed techniques to observe the dynamics of individual protein molecules on the cell surface. Thus, we developed a technique to do high precision simultaneous tracking of individual fluorescently labeled receptors and small receptor clusters using quantitative digital video fluorescence microscopy (Ghosh and Webb, 1988, 1989, 1990). We first developed this technique for the low density lipoprotein receptor (LDL-R) system (Brown and Goldstein, 1986), and have subsequently generalized it to be an applicable tool for other cell surface receptor systems (Slattery et al., 1991). We have found that looking more closely at the motion of discrete individual cell surface receptor molecules is a powerful technique to probe the nature of the constraints to their motions, without the limitations of FPR (Ghosh et al., 1986; Ghosh, 1991; Ghosh and Webb, 1990, in preparation). This approach also reveals if receptors on different areas of the cell move differently, and how they move with respect to other cellular structures (Ghosh and Webb, 1987, 1988, 1989, 1990, 1991, in preparation).

Development of the technique of automatically and simultaneously tracking the motion of individual low density lipoprotein receptor molecules (LDL-R) with high localization precision posed various experimental and theoretical challenges. The methodologies we developed are described in this paper. Results from using these techniques are presented elsewhere (Ghosh and Webb, 1990, in preparation; Ghosh, 1991; Slattery et al., 1991; Brust-Mascher et al., 1992, 1993).

LDL-R system

Our ability to label, localize, and track individual LDL-R molecules on cell surfaces was made possible by the development of the extremely fluorescent, biologically active form of LDL, diI-LDL (Barak and Webb, 1981). LDL is a 22 nm diameter sphere coated by a mono-molecular layer of phospholipids and cholesterol around a hydrophobic core filled with cholesterol esters. The single protein, apoprotein B-100 in the surface monolayer tightly binds LDL to its receptor with a 1:1 stochiometry (equilibrium dissociation constant $K_d = 2.5 \times 10^{-9}$ M) (Innerarity et al., 1980; Pitas, 1979). In normal cells the LDL-R is clustered in coated pits and internalized whether or not LDL is bound to it. Tracking was done on two human fibroblast lines expressing mutant LDL-Rs with differing cytoplasmic tail sequences that do not cluster in coated pits or undergo receptor-mediated endocytosis (Brown and Goldstein, 1986). These internalization-deficient cell lines were used so that the LDL-Rs remained on the cell surface while we tracked them. This system of cell and mutant receptor provides an archetypical example of cell surface receptor mobility and motility that provides the basis for an extended series of studies of cell surface receptor dynamics.

Although the size of the LDL particle is much smaller than the diffraction-limited resolution of an optical microscope, the bright fluorescence emission of diI-LDL enables us to localize the position of LDL-R molecules on the cell surface with much sharper precision than the resolution-limited image of the marker. This high precision of location is made possible by the natural scarcity of the LDL-R on the cell surface; there are only about one thousand LDL-Rs per cell (~1 LDL-R molecule per μm^2). The small number density of receptors makes possible the resolution of the discrete punctate staining pattern representing individual LDL-R singlets and small clusters. Microscope resolution limits the resolvable marker number density to less than 1 per μm^2.

The first studies of LDL-R motion were conducted by Barak and Webb (1982) using the technique of FPR with a bleached stripe pattern instead of a spot in order to collect enough fluorescence signal from the sparse density of diI-LDL stained receptors. Their ensemble-averaged diffusion data showed that at temperatures above 21°C, LDL-Rs diffuse very slowly on JD cells (an internalization deficient cell line) at 1.4 to 4.5 $\times 10^{-11}$ cm^2/s with the mobility attributed to 60–80% of the receptors. Because the diffusion was so slow, defining a mobile fraction was difficult. As will be shown, this problem is alleviated by the tracking of single LDL-R molecules with high localization precision.

Barak and Webb also induced the cells to form blebs that separated the cell membrane from the cytoskeleton. Here LDL-R diffusion was also measured and found to be very fast. To do this measurement, a low light level image-intensified video camera attached to a microscope was used to record on videotape a series of real time fluorescence images showing the punctate indications of individual receptors and clusters. Clear acetate sheets were placed over the TV monitor images of the time-lapse video recording, and the particle positions over time were tracked. Calculating the mean-squared displacement from their position versus time data and fitting them with a straight line yielded diffusion coefficients of the order of 10^{-9} cm^2/s for LDL-Rs on blebs. The LDL-Rs seemed to be undergoing random Brownian motion as indicated by the linear fits of these early molecular tracking data.

Computer-assisted tracking was developed further by Gross and Webb (Gross and Webb, 1988; Webb and Gross, 1986). This tedious plotting technique for analyzing particle displacements over time has been reconstructed into our current computer-automated tracking techniques capable of routine simultaneous, automated tracking of thousands of molecules with a spatial precision of about 30 nm at one image per s (Ghosh and Webb, 1988, 1989, 1990, in preparation; Ghosh, 1991). Automated tracking is important because it allows a large number of particles to be tracked easily, enabling trends in cell surface particle motions to become more apparent due to the reduction of statistical variations between trajectories, as implicitly demonstrated by the probability density distributions and other statistics used by Saxton in his computer simulations of diffusing particles (Saxton, 1993). Elsewhere, we demonstrate this and show how we determine

differences between diffusive and directed motions of LDL-Rs (Ghosh, 1991; Ghosh and Webb, in preparation). Anderson et al. (1992) have also recently reported studies of LDL-R tracking.

MATERIALS AND METHODS

Introduction to automated tracking

A tracking experiment first requires the staining of LDL-Rs with dil-LDL on a mutant internalization-deficient human fibroblast cell to visualize the individual receptors. The acquisition of up to 1000 images at data rates to 3 Hz with negligible photobleaching was achieved using either a low light level image-intensified video camera or a low light level Charge Coupled Device (CCD) camera. The images are digitized, stored, and later analyzed in an image processor that recognizes, locates, and tracks the individual fluorescently labeled receptors from image to image and consequently yields the precise receptor trajectories over trajectory times up to 45 min. Of course once a zoo of single particle trajectories were obtained, their data must be readily processed and analyzed to be interpreted and understood.

The automated tracking program enabled several hundred particles to be recognized simultaneously, precisely located, and tracked through many images, usually 100–1000 frames, without the need for user interaction. Automated tracking of LDL-Rs involves the iterative application of two key steps. The first identifies LDL-Rs in the current image, and the second matches LDL-Rs found in the previous frame with those in the current frame. The particle's position was defined as the weighted center of mass of its image over the pixels it covered. Thus, each particle's location was determined from the mean of the pixels' positions weighted by each pixel's intensity, for the pixels occupied by the particle. A ciné picture of the global patterns of motion and trends on the cell surface is obtained from these data, and is displayed with comparative ease. The digital data on the coordinates of each of these particles versus time are also available for more detailed analysis of particle micro-motions and particle-particle correlations.

Image acquisition

Time-lapse fluorescence images of the dil-LDL-stained cell are taken at 37°C with a low light level camera. Most of the experiments used a KS-1380 microchannel plate intensifier (Videoscope International, Washington, DC) coupled to a silicon diode 67-M video camera (Dage-MTI, Michigan City, IN) on a Zeiss inverted IM-35 microscope (Oberkochen, Germany). A few experiments were also done using a Photometrics cooled Charge Coupled Device (CCD) camera with a Thompson 7882 chip and 14-bit digitization with 50-kHz readout (Photometrics Ltd., Tucson, AZ) on a Zeiss Universal upright microscope.

Samples were epi-illuminated by a 100 W Hg arc lamp. The light from the Hg arc lamp was first reflected off a cold mirror to remove infrared light. It was then passed through a narrow band 546 nm interference filter to select the 546 excitation light. This was then focused onto the entrance window of a 1 m long liquid light pipe, 18 mm in diameter (Oriel, Stratford, CT). The light pipe is used to smear out the image of the Hg lamp arc to provide spatially uniform illumination intensity. A mechanical, computer-controlled shutter with a 6 ms opening time (Vincent Associates, Rochester, NY), was placed after the exit window of the light pipe, just before the epi-port of the microscope. The exit window of the light pipe and the microscope's epi-iilumination system are adjusted for Koehler illumination.

We used a 1.25 numerical aperture, 100X, Phase Contrast 3, oil immersion Zeiss objective. Zeiss immersion oil (518C) with index of refraction 1.518 was used. A 565 nm dichroic mirror and a 590 nm interference barrier filter selected the dil fluorescence emission to reach the camera. The excitation filter (546DF10) and the barrier filter (590DF35) were from Omega Optical (Brattleboro, VT), and the dichroic mirror was from the Zeiss FT-580 dichroic mirror pack. A highly reflective sliding mirror diverted the image from the binocular eyepieces to the camera port, which contained an $f = 100$ mm Zeiss projection eyepiece coupled to an $f = 63$ mm Zeiss C-mount camera objective.

Temperature was maintained by an air-stream incubator (Nicholson Precision Instruments, Bethesda, MD) and monitored using a thermocouple probe attached to the microscope objective. Evaporation was prevented from the specimens, because their chambers were sealed.

The images were digitized, stored, and analyzed by a Trapix 5500 image processor (Recognition Concepts Inc., Carson City, NV) run by a microVAX-II minicomputer (Digital Equipment Corporation, Maynard, MA). The digitization was done by an 8 bit A/D converter. Fast acquisition and storage of images (e.g., 0.6–3 Hz) was made possible by a digital real time hard disk of 1.2-Gbytes capacity. The sample was continuously illuminated while frames were digitized, averaged, and then stored on the real time disk. Slower acquisition rates (e.g., 0.07–0.02 Hz) employed the computer-controlled shutter to illuminate the sample intermittently only during image acquisition.

A dark current image, where no excitation illumination was present, was taken with each experiment. To measure and correct for the ambient background, an image was also taken of a slide containing only phosphate-buffered saline (PBS). This background image was subtracted from the dil-LDL images. For experiments on cells, a phase-contrast image was taken before and after the experiment, to record any gross changes in cell morphology.

Time-lapse sequences of images taken on the real time disk were either sets of 900 unaveraged frames taken at 3 Hz or 150 images, each an average of 32 frames, taken at 0.6 Hz. This translates to a total length of time for each image set of 5 and 4 min, respectively. For slower acquisition rates, time-lapse image sets spanned a time of 30 to 45 min, with each image being an average of 32–256 frames.

Tracking algorithm

TRACK, the automated tracking program we developed, is written in Fortran 77. It uses Fortran image processing subroutines for the Trapix developed by Tau corporation (Los Gatos, CA.).

At the beginning of the program, the trackball-controlled cursors are used to select the region in which the particles are to be tracked. The selected box can be of any size, and can include the entire 512×480 pixel image.

To identify the particles to be tracked, TRACK calls two subroutines: CLEANUP and GETCOORD. CLEANUP spatially filters the image of a dil-LDL-stained cell so that a mask of the fluorescent spots is created. GETCOORD uses this mask to identify each particle, and then computes the center coordinate and power of each of the spots. CLEANUP spatially filters an image by first doing a convolution with a 5×5 Laplacian filter to remove the local mean (i.e., equivalent to high pass filtering) (Inoue, 1986). Then the image is convolved by a similar sized smoothing filter to get rid of artifacts from high pass filtering not associated with particles. These convolution kernel dimensions were empirically determined to yield the clearest spatially filtered masks of dil-LDL images. The image is then sliced above a threshold intensity in GETCOORD to remove any remaining background, and to improve resolution for particles close to each other. If two particles are close to each other and are barely resolvable by eye on the image frame, local mean removal followed by smoothing causes the two particles to appear fused as one. The saddle joining the two particles is of a lower intensity than the intensities at the centers of the particles if they are far enough to be resolved. Thresholding gets rid of this low intensity saddle, and the two particles appear distinct, but are subject to a position error introduced by the overlap of the particle images. The threshold level that will work the best is interactively determined, and then entered by the user at the beginning of the program. Clearly, the errors of position due to overlap (<20% of particles) and ambiguity of particle identity are minimized by low particle density, a fortunate characteristic of the cell system studied.

GETCOORD uses three image planes that for descriptive purposes we will call 1, 2, and 3. Image plane 1 contains the original fluorescence image. The spatially filtered image from CLEANUP is placed in image plane 2. Image plane 3 is initially zero. To slice the image above threshold, any pixel value in image plane 2 that is greater than the threshold value is assigned a constant nonzero value in image plane 3. Image plane 3 thus contains the map of the thresholded image. Another routine then looks at image plane 3 and determines which of the nonzero pixels are contiguous, thus defining

the area covered by one particle. The mask in image plane 3 is used to identify each individual particle in image plane 1, along with its power. Thresholding is used to eliminate background and can be a source of error at high background levels resulting from high particle densities.

For images acquired with the video camera-intensifier system, each pixel is 200 nm in width, and the entire imaged dil-LDL spot is encompassed by about 8×8 pixels. A cross section through the point spread function, which determines the image profile of the point source, resembles the Airy pattern expected from the diffraction of a point source by a circular aperture. Finding the weighted center of mass of a dil-LDL spot's image over the pixels it covers enables us to determine the particle's location with a precision better than the dimension of a single pixel. To determine this center of mass, the x coordinate of each pixel imaging the dil-LDL spot multiplied with the intensity at that pixel is summed over all the pixels imaging the spot, and then normalized by the sum of the intensities of the pixels, giving the x center of mass, and the y position is similarly determined. The fluorescence power of each particle is also determined.

The tracking is carried out by a subroutine called TRACKER, which uses a routine called BOXES that goes to the location of each particle in the $i - 1$ frame (i.e., the previous frame) and draws progressively larger squares around it until it finds a particle in the current frame within this square. The box is allowed to expand until either a particle is detected within it, or the maximum allowable diffusion radius is reached, which is calculated from an upper bound diffusion coefficient and time entered by the user at the beginning of the program. If no particle is found in the square to match up with the particle in frame $i - 1$, then this particle is entered into a storage matrix.

After all the particles in frame $i - 1$ have been either matched up with a particle in the current frame or placed in the storage matrix, a similar storage matrix, created when frame $i - 1$ was the current frame, is searched. The particles in this older storage matrix are compared to particles in the current frame to see if they match using BOXES. This is done because a particle may briefly disappear from one frame and reappear in the next. This safety system of storage matrices tries to ensure that particles are not lost. However, if particles cannot be matched after two frames, they are assumed lost. Any remaining particles in frame i that have not been matched up are assumed to be new particles and, thus, are entered in the record. New particles can have several origins: two pre-existing particles that fuse will be recorded as a new particle; a particle moving in from an area outside the selected region being tracked will be registered as a new particle. If a particle, due to cell topography, was outside the current field of focus, it would be too dim to register as a particle. However, when it descended into the field of view and came into focus, it also would be recorded as a new particle.

The user can also specify that only particle trajectories that lasted longer than some minimum number of images be retained. This guards against briefly occurring noise or other imaging artifacts. Another option exists, whereby GETCOORD will only act upon those spots containing more than a minimum number of pixels. Specifying a minimum number of imaged frames for a particle also selects against these artifacts. TRACK thus reviews all its particle trajectories, and saves and stores only those trajectories longer than the user specified time.

Two dil-LDLs whose separation in an image is less than the light microscope's resolution will appear as one particle. Determining the optical center of mass of this one particle with a precision better than the size of 1 pixel (200 nm) will give a position that is displaced from the true positions of the two individual dil-LDLs. If the two unresolved particles are linked to each other and move as one entity, the position determined from the center of the Airy pattern represents the center of the cluster and is a valid position coordinate. If the two individual particles' motions are independent of each other, then their separation in future frames will eventually increase to a distance greater than the microscope's resolution, enabling the separate localization of both particles. If two independent particles met and stuck together making a larger particle, one of the old particle's trajectories would be lost, and the trajectory of the new larger particle would appear as a continuation of the other old particle's trajectory. The particles' spacings are larger than the amount they move between time frames, thus mistaking one particle for another while tracking is rare (<5% of the particles on a cell for the entire time-lapse sequence).

TRACK stores the coordinate versus time information for each particle. This data file can now be accessed by other analysis programs.

Making DiI-LDL

LDL was isolated from human plasma (Red Cross Blood Bank, Syracuse, NY) using the method of KBr density centrifugation described by Goldstein et al. (1983), or purchased from Chemicon International (Temecula, CA). LDL was stored under an inert gas (argon) atmosphere in 0.01% azide. LDL protein was measured with a protein assay kit obtained from Sigma Chemical Co. (St. Louis, MO) using the modified micro-Lowry procedure of Peterson (1977). DiI-LDL was made by the method of Barak and Webb (1981) (Ghosh, 1991), and stored under argon, at 4°C, in the dark. An alternative method of making dil-LDL was described by Pitas et al. (1981). Some dil-LDL batches made by our method were also obtained from Molecular Probes, Inc. (Eugene, OR).

Cell culture, labeling, and testing of DiI-LDL

To test dil-LDL labeling of its receptor on cells, and to do cell tracking and clustering experiments, we grew four human skin fibroblast lines. These are: (i) GM3348 normal human fibroblasts; (ii) GM2000 mutant fibroblasts that do not express cell surface LDL-Rs; (iii) GM2408A, or JD; and (iv) FH683. The first three cell lines are from the NIGMS (National Institute of General Medical Sciences) Human Genetic Mutant Cell Repository (Camden, NJ), and FH683 was the kind gift of Drs. Michael Brown and Joseph Goldstein (Brown and Goldstein, 1986). The three mutant fibroblast lines are from patients with familial hypercholesterolemia (FH) and have been characterized by Brown and Goldstein (1986). GM3348 and GM2000 lines were used as positive and negative controls, respectively, to test for dil-LDL binding specificity, whereas tracking experiments were done on the internalization deficient GM2408A and FH683 lines.

The cells were grown in Dulbecco's Modified Eagle's Medium (DMEM) (Gibco, Grand Island, NY) supplemented with 10% v/v FCS and 20 mM HEPES. Cell lines were cultured in 75-cm^2 flasks (Corning Medical, Corning, NY) at 37°C in a humidified 5% CO_2 atmosphere incubator. For experimental use, cells were plated, on day 0, onto 22 mm^2 number 1 coverslips at a density of 8×10^4 cells/dish, in a 60×15 mm polystyrene petri dish with two coverslips per dish. Media was replaced with fresh media on day 3, and on day 5 the media was changed to DMEM with 20 mM HEPES and 10% delipidated FCS, to upregulate cell surface LDL-R numbers. Cells were ready to use on day 7 and were used until day 10. Cells with high passage numbers ($\geq$20) were discontinued and discarded. Delipidated FCS was made by the method of Goldstein et al. (1983).

Cell labeling for tracking experiments was done at 4°C, and all reagents were chilled before application. The coverslip was washed twice with Medium 199 without phenol red (Gibco) and supplemented with 10 mM HEPES, pH 7.4 (Buffer A). It was then incubated in 10 μg/ml dil-LDL in Buffer A for 15 min. The coverslip was rinsed twice and then incubated with PBS (Gibco) containing 2 mg/ml BSA (Sigma) for an additional 15–30 min, to remove nonspecific labeling. After washing twice more in Buffer A, the coverslips were mounted on a glass microscope slide and sealed with a 1:1 mixture of paraffin and Apiezon wax (Apiezon Products, U.K.), which provides a firm sealant at 37°C. The cells were then observed under the microscope. For testing dil-LDL binding to GM3348 and GM2000 cells, the cells were rinsed twice in PBS and then fixed for 5 min in 3.8% formaldehyde in PBS at room temperature. The cells were again rinsed twice with PBS and then stained as above, except at room temperature.

We checked the structural integrity of dil-LDL by looking at its negatively stained electron micrographs, as described before (Barak and Webb, 1981). To confirm the presence or absence of LDL-Rs on our cultured cells, we did indirect immunofluorescence using a rabbit polyclonal anti-human LDL-R antibody (the kind gift of Dr. Richard Anderson, University of Texas Health Science Center, Dallas, TX).

We saw no dil-LDL staining on GM2000 fibroblasts, whereas bright punctate staining was seen on the other three cell lines. DiI-LDL labeling was prevented by the presence of an excess of unlabeled LDL (Barak and

Webb, 1981). Thus, dil-LDL binds specifically to the LDL-R. The equilibrium dissociation constant of LDL from its receptor is $K_d = 2.5 \times 10^{-9}$ M, and the rate constant for dissociation is 6.3×10^{-5} s^{-1} (Innerarity et al., 1980; Pitas, 1979). LDL and dil-LDL have the same equilibrium dissociation constant from the LDL-R (Pitas et al., 1981). Thus, dil-LDL is tightly bound to its receptor during the course of our experiments.

RESULTS

Nanometer precision and limitations

Introduction to high precision localization

DiI-LDL is assumed to act as a point source because the pixelated image of a single dil-LDL molecule represents the expected point spread function Airy pattern from the diffraction of a point source by the circular back aperture of the objective lens. The center of mass of this symmetrical point spread function can be localized with a precision limited by neither the size of the data pixels recording the image (with a sufficient number of pixels in the image) nor by the diffraction limited breadth of the image. However, the actual precision in localizing a particle depends on the noise characteristics of our image detector system, which has to be measured, on shot-noise uncertainty in the images and on any inhomogeneity of background. Nonuniform background would also affect the accuracy in localizing a particle, and may limit the resolution of detection and the observation of systems with large particle densities. This is not a problem in our system where we have relatively flat background and low particle densities. We will demonstrate that our present system can simultaneously and automatically localize and track thousands of dil-LDL with a precision of 30 nm with about 1 s measurement time per image (Ghosh and Webb, 1989). There remains a potential opportunity for an order of magnitude improvement of precision for comparable preparations in future developments. The precision improves as the signal-to-noise ratios increase, the background is eliminated, and mechanical stability is improved.

Determining localization precision

To determine the limits to our precision, we scattered dil-LDL particles on a microscope slide where they stuck to the glass surface and remained immobile. We recorded a sequence of time-lapse images in the same manner as for cells (imaging rate of 3 Hz) and then tracked the immobilized particles. The trajectories of two dil-LDL particles on the same slide, for 2.25 min, are shown in Fig. 1. Pseudo-color of the pixels in Fig. 1 represents the time evolution of the tracked positions going from dark blue to red. We find that the microscope system has an apparent slow drift during this time with a net displacement of 140 nm from the starting position.

To measure the drift and to correct for it in measuring tracking precision, we subtracted the coordinates of pairs of neighboring immobilized particles on the same slide and plotted the difference positions at the different times for the particle pair in Fig. 1, in Fig. 2. The SD of this distribution of differences divided by $\sqrt{2}$ gives the limit of precision, with the assumption that the remaining

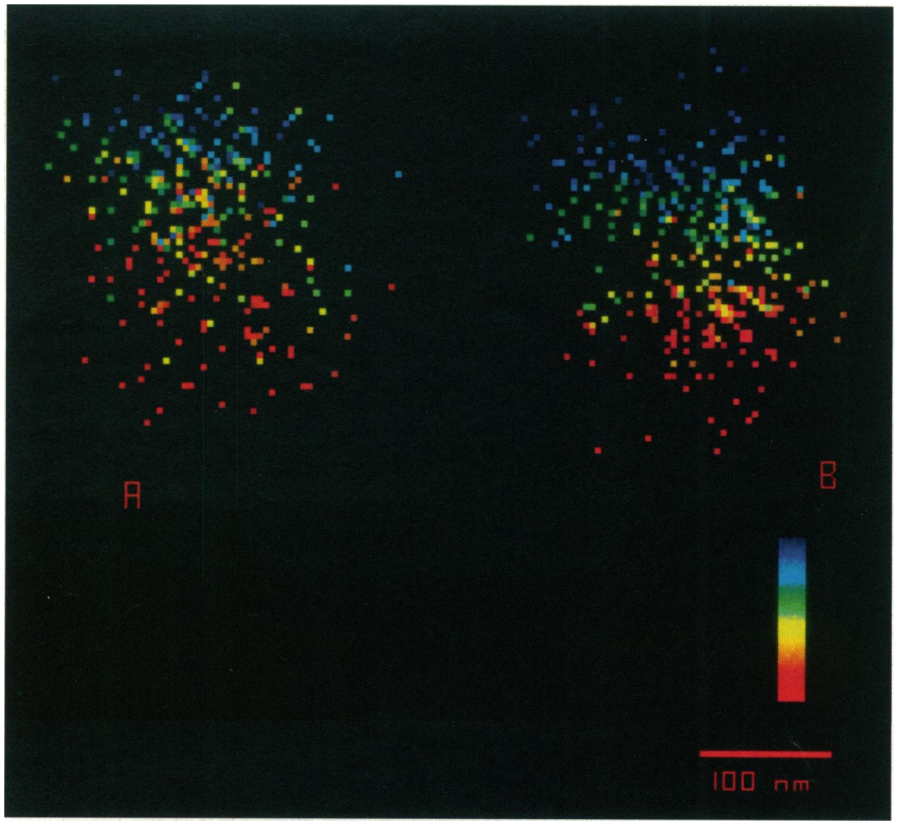

FIGURE 1 Trajectories of two immobilized dil-LDLs on a slide (labeled A and B), showing the slow drift of the system. The pseudo-color represents the time evolution of the positions with starting time depicted in dark blue, and the position in the last frames in red. Time ≈2.5 min, and the system was displaced ≈140 nm in this time.

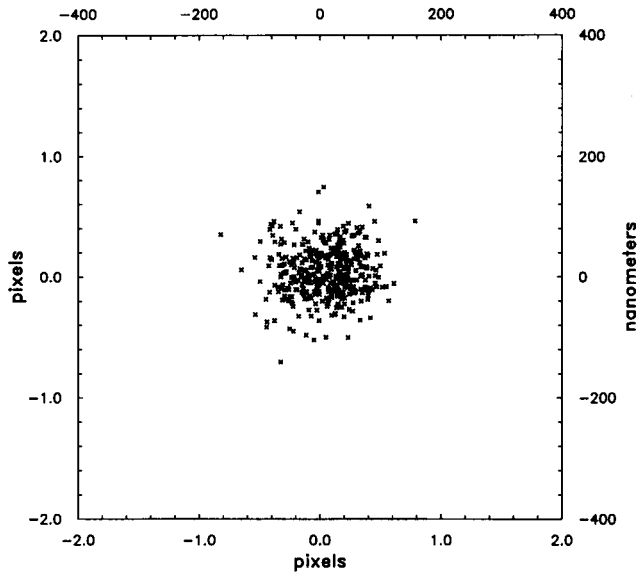

FIGURE 2 Immobilized dil-LDL positions corrected for drift. The coordinates of the two particles in the previous figure were subtracted from each other at each time point to give this difference distribution of particle positions. The tracking precision is defined as the SD of this distribution of positions divided by $\sqrt{2}$, which gives a precision of 30 nm.

apparent displacements of the individual immobilized particle positions are uncorrelated. This measure yields a precision of 30 nm for the video camera-intensifier system. We have measured this level of precision about 15 times, using our two standard imaging conditions (each image being either the average of 10 frames or 32 frames, and an exposure per frame of 33 ms), and it is a consistent and reproducible result.

Another determination of tracking precision analyzes the apparent displacements of the immobilized particle in the time between two sequential images. This displacement is due to both slow drift and the measurement uncertainty in localizing a particle. However, the dominant contribution is due to the uncertainty in position measurement, and slow drift is rarely a problem (see below). The root mean square displacements between successive images also gives a tracking precision of 30 nm, with the standard conditions. In the standard conditions the sample was continuously illuminated while image frames were continuously digitized at video rate (33 ms exposure per frame), the images recorded during either 1 or 0.33 s were averaged, and then stored on the real time disk at a rate of either 0.6 or 3.0 Hz. The duty cycle was thus about 1.6 or 0.33 s per stored image, respectively.

The slow drift of the microscope system in a typical 4-min experiment (~200 nm) is small compared to the scale of LDL-R motion on JD cells, which covers several micrometers in the same length of time. Thus, in measurements on cells, fiducial drift has rarely been a problem. This is illustrated for typical cases by plotting the logarithm of an immobile particle's mean-square displacement versus the logarithm of the time interval over which the displacement was measured, and comparing it to a similar analysis done on a diffusing LDL-R tracked on a JD cell, as shown in Fig. 3. The mean-squared displacements for the immobile particle at 1 s is 10 times less than for the LDL-R on the cell and at the maximum time interval recorded for the immobile particle in this plot (70 s) the LDL-R on the cell moved more than 1000 nm, whereas the immobile particle had a total displacement of 140 nm.

A plot of the mean-squared displacement versus time interval τ for the immobile particle shows nonzero mean-squared displacement at a time interval of zero due to the existence of the measurement uncertainty. At large time intervals (>10 s), the system's drift looks diffusive because it can be roughly fit by a straight line, yielding an apparent diffusion coefficient $D = 5.3 \times 10^{-13}$ cm^2/s (not shown). From $\tau = 0$ the localization sensitivity $\sqrt{\langle \Delta r^2 \rangle / 2} = 30$ nm.

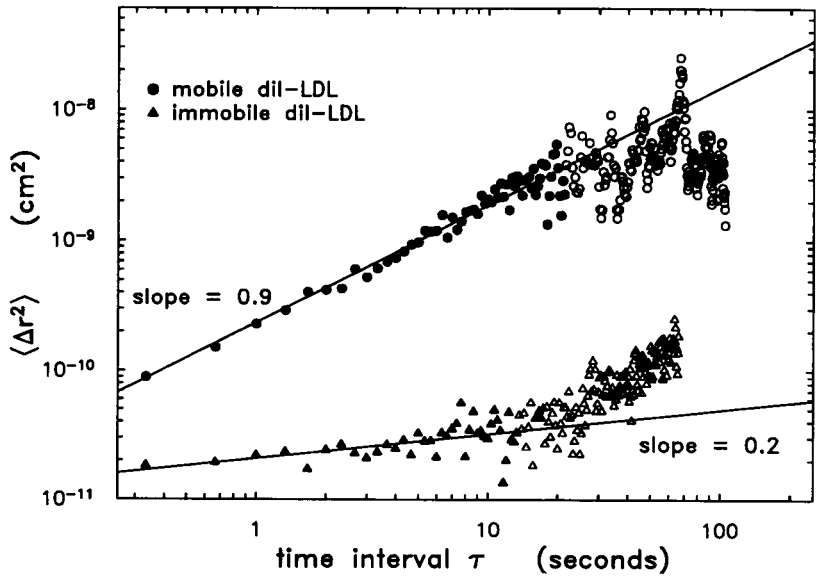

FIGURE 3 Log mean squared displacement versus log time interval plot for an immobile test particle (*triangles*), and a diffusing LDL-R (*circles*) on a cell. The slopes are fit to the filled symbols.

For short time intervals in these data the measurement uncertainty (30 nm) dominates the effects of drift ($\sqrt{2D\tau}$ = 13 nm) in determining the position uncertainty.

Characterization of detected noise

To examine further the nature of our ability to localize point objects, we examined the signal-to-noise characteristics of our camera-intensifier detector system in the manner of Ryan et al. (1990). Signal-to-noise was measured by first acquiring 150 images of a uniform thin target at 1.6-s intervals, each one an average of 32 frames. Sets of images were taken of an optically thin film of dil uniformly distributed in DMSO, at a variety of illumination intensities, provided by neutral density filters.

The sample showed minimal bleaching, so was treated as a time-independent ensemble. Assuming a sample-independent geometrical loss factor in the optics, the mean number of detected photons, $\overline{\mathcal{N}}$, is proportional to the mean number of photons emitted by the sample. The camera has a linear response, so the mean pixel intensity is proportional to the number of detected photons (Ryan et al., 1990). Thus, we can write

$$\overline{\mathcal{N}} = \mathcal{K}\bar{I}, \tag{1}$$

where $\mathcal{K}$ is the proportionality constant.

The SD of the pixel signals over time (noise), σ, was plotted against the mean pixel signal, $\bar{I}$, on a log-log plot in the manner of Ryan et al. (1990), and was fit to a straight line

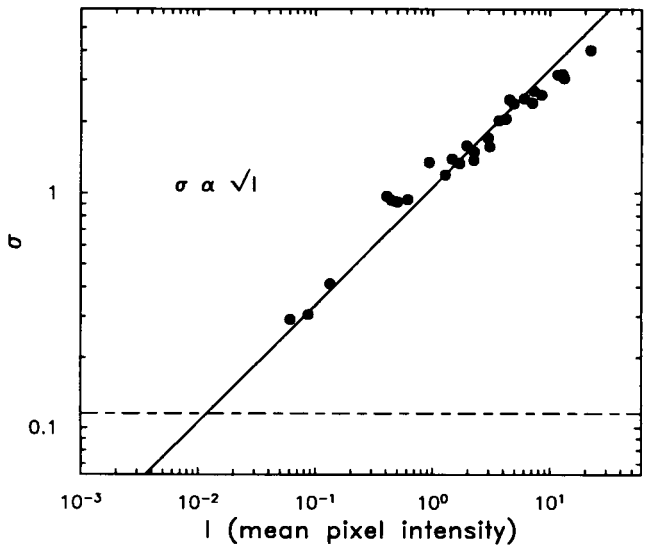

FIGURE 4 Signal shot-noise. The logarithm of the SD of the fluctuations in detected signal in ADU (Analog to Digital Units) from a pixel, σ, is plotted versus the logarithm of the mean of this signal, I. The data were fit with a straight line giving a slope 0.5, implying the signal is shot-noise limited. The dashed line corresponds to the measured dark current fluctuations. From the intercept of several measurements, we determine that the number of photons detected above noise is 1.5 times the mean pixel signal in ADU.

giving a slope of 0.5, shown in Fig. 4. We write this as

$$\sigma = \sigma_1\sqrt{\bar{I}}, \tag{2}$$

where σ_1 is the value of σ when $\bar{I} = 1$. This relation implies that the usefulness of the signal, $\bar{I}$, is limited by shot noise, where the signal-to-noise ratio increases as $\sqrt{\overline{\mathcal{N}}}$. The actual signal measured, $\bar{I}$, is the sample's signal plus the background from the dark current. The dark current level is measured by imaging a sample, in the same manner as before, except with no excitation illumination. Thus, the net signal from a sample is

$$\bar{I}_{\text{net}} = \bar{I} - \bar{I}_{\text{DC}} \propto \overline{\mathcal{N}}, \tag{3}$$

where $\bar{I}_{\text{DC}}$ is the dark current signal. The net noise is

$$\sigma_{\text{net}} = (\sigma^2 - \sigma_{\text{DC}}^2)^{1/2} \propto \sqrt{\overline{\mathcal{N}}}, \tag{4}$$

where σ_{DC}^2 is the dark current variance, and σ_{DC} and σ_{net} are assumed to be uncorrelated. Thus, the signal-to-shot-noise ratio is

$$\frac{\bar{I}_{\text{net}}}{\sigma_{\text{net}}} = \sqrt{\overline{\mathcal{N}}}; \tag{5}$$

squaring this, we can determine the number of detected photons as

$$\overline{\mathcal{N}} = \left(\frac{\bar{I}_{\text{net}}}{\sigma_{\text{net}}}\right)^2 = \frac{(\bar{I} - \bar{I}_{\text{DC}})^2}{(\sigma^2 - \sigma_{\text{DC}}^2)}. \tag{6}$$

As Ryan et al. (1990) point out, this provides a lower boundary for the actual number of photons detected, because other noise contributions with similar square-root dependencies on $\bar{I}$ may exist.

The mean number of photons can also be determined from $\bar{I}$, by using Eqs. 1 and 2 and the fact that the SD of the number of photons is equal to the SD of the intensity fluctuations times the same proportionality constant $\mathcal{K}$. Solving for $\mathcal{K}$, we find that

$$\mathcal{K} = \frac{1}{\sigma_1^2}. \tag{7}$$

Examining σ_1 for several pixels, we find that $\mathcal{K} = 1.5 \pm 0.7$. Thus, the main limitation to determining the power from a single dil-LDL will be the shot noise associated with its photons and the neighboring ambient background.

Limitations to tracking precision

We expect the tracking precision to vary reciprocally with the signal-to-noise ratio of the particle image as

$$\sqrt{\frac{\langle \Delta r^2 \rangle}{2}} = \frac{\langle W \rangle \sigma}{\bar{I}} = \frac{\langle W \rangle}{\sqrt{\mathcal{S}}}\sqrt{\frac{\mathcal{S} + \mathcal{B}}{\mathcal{S}}}, \tag{8}$$

where $\sqrt{\langle \Delta r^2 \rangle / 2}$ is the precision, σ and $\bar{I}$ are the SD and mean of the fluorescence power, respectively, of the photon flux density distribution over the entire spot, $\langle W \rangle$ is the radius

of the base of the imaged spot, $\mathscr{S}$ is the number of signal photons in ADU (Analog to Digital Units), $\mathscr{B}$ is the number of photons from the background in ADU, and $\sqrt{(\mathscr{S}+\mathscr{B})/\mathscr{S}}$ is the noise correction factor to account for the noise contribution from the background photons $\mathscr{B}$. If there were no background, the signal-to-noise would be the shot-noise-limited signal $\sqrt{\mathscr{S}}$. However, in our experiments, in addition to signal photons from the particle, there are photons from the background that also have a shot-noise dependence. Although we subtract the background from the signal in experiments, the background noise contribution cannot be ignored, and hence the extra term in Eq. 8.

To test experimentally Eq. 8, monodisperse 93 nm fluorescent, carboxylated latex microspheres (Molecular Probes) were spread at low number density onto a slide. Sets of time-lapse images at different illumination intensity levels, were acquired for each bead, and the precision (root mean-squared displacement at the shortest time interval) was determined. The mean fluorescence power over time, and the SD of the power were also computed for each bead.

Plotting the signal-to-noise (i.e., mean fluorescence power per particle divided by SD) versus the precision gives a hyperbolic-looking curve (see Fig. 5), where the smaller (better) precision occurs at larger signal-to-noise. The theoretical curve from Eq. 8 was also plotted, where a typical experimental background level of $\mathscr{B} = 25$ ADU was used, and the characteristic width $\langle W \rangle = 800$ nm, the typical width of the base of our imaged spots (i.e., the first zero of the Airy pattern). A precision of 30 nm is measured at signal-to-noise of 6 to 12. Monomeric dil-LDL has a signal-to-noise of about 6 under these conditions (shown later), giving a precision around 30 nm. For a signal-to-noise less than 6, the precision worsens precipitously. The theoretical curve, which accounts for shot-noise limited signal with a typical shot-noise background, matches the experimental curve at low signal-to-noise. At higher signal-to-noise, however, the precision improves slowly, and appears to encounter a barrier against better localization at around 15 nm (corresponding to a signal-to-noise value of about 20). This confirms the earlier observation that at low measurement uncertainty (due to high signal-to-noise), the system drift is the main contribution to localization precision, and this drift was 13 nm for a 1.6 s time interval between frames. Thus, as signal-to-noise improves, so does the tracking precision until the drift contribution of the system between two subsequent frames is larger than the measurement uncertainty from shot noise. Better tracking precision is obtained by both improving the particle's signal-to-noise and reducing system drift.

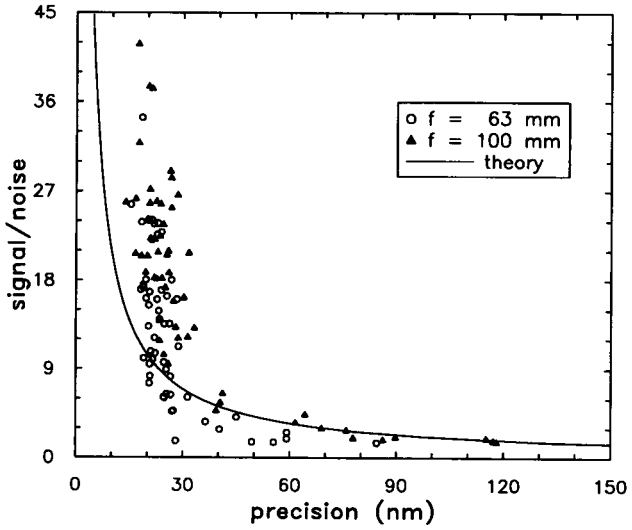

FIGURE 5 Dependence of particle tracking position uncertainites (precision) on image signal to noise ratio. The experimental results seem to encounter a limit of precision around 15 nm at high signal-to-noise where they depart from the theoretical curve of Eq. 8. Signal-to-noise ratios for images of an immobilized 93-nm bead versus the root-mean-square tracking precision, for magnified (f = 63 mm projective eyepiece, *circles*), and demagnified (f = 100 mm, *triangles*) images are plotted. The solid line is the theoretical prediction from a shot-noise limited signal, and background, where a typical experimental background of 25 ADU was used. DiI-LDL has a signal-to-noise around 6, giving a 30 nm tracking precision.

These experiments were repeated using a 63 mm focal length projective lens instead of the usual 100 mm focal length projective lens to magnify the bead's image and spread it over a larger number of data pixels on the camera faceplate (increase $\langle W \rangle$ in Eq. 8). This had little effect on tracking precision and gave similar results to the $f = 100$ mm case shown in Fig. 5, as was expected. Although magnifying the image decreases the signal-to-noise per pixel, the proportionate increase in the number of pixels contributing to the image exactly compensates. Pixelation error is unimportant in the precision of location of a symmetric image.

Computer simulations confirmed the result that signal-to-noise is proportional to the reciprocal of the precision (Ghosh, 1991) and is similar to the result obtained analytically for a general resolution and noise-limited instrument by Bobroff (1986). Magnifying and demagnifying the image in the simulation gave identical signal-to-noise versus precision curves, as we saw experimentally.

Single DiI-LDL recognition and detection

Detection and recognition of single LDL-R molecules

Although the imaged size of the digitized fluorescent spot corresponding to an LDL particle is determined by diffraction and does not reflect the actual size of the source it represents, the total fluorescence power of each spot is indicative of the number of LDL-Rs in the spot. Thus, the power of each fluorescent spot yields a measure of the number of unresolved receptors that are clustered in it.

Gross and Webb (1986, 1988) measured the fluorescent power distribution of single and clustered dil-LDL particles bound to their receptors. They fit this distribution with a multiple Poisson probability distribution function. Assuming Poisson statistics for the loading of LDL by the dil fluorophore, they showed that the width of the first distribution peak gave n, the mean number of dils in monomeric dil-LDL. The batch of dil-LDL they used had 40 dil fluorophores per LDL. The mean power of higher power peaks in the

distribution were integer multiples of the monomer peak's power, indicating the distribution of LDL-Rs into a distribution of small clusters. Further details of this method is described in length elsewhere (Ghosh, 1991).

To determine whether the fluorescent spots identified as single diI-LDLs from the multiple Poisson fitting were really singles we determined n, the mean number of diI's in monomeric diI-LDL, by three different methods and compared the results with the n obtained from multiple Poisson fitting. The first of these methods used spectrophotometry, where we compared the absorbance of diI-LDL with that of diI. The other two methods for determining n were based on microspectrofluorometry within the photometric microscope. We first obtained n by normalizing the fluorescence power obtained from individual diI-LDL particles on a slide by the power density obtained from a thin film of known concentration of diI in a solvent. The second microspectrofluorometry method normalized the number of photons from single diI-LDL particles by the number of photons from diI in a thin film. The numbers of detected photons were determined by measuring the variances in the shot-noise limited signal measured on our equipment. The results from these methods confirmed our ability to detect readily the single diI-LDL particles and to count the number of unresolved diI-LDLs in larger clusters (containing up to 5–7 diI-LDLs).

A dilute sample (~0.1–1 μg/ml) of diI-LDL was placed on a microscope slide, covered by a coverslip, sealed, and then a time-averaged image of the field of adhered particles was taken. This dilution gave a discrete, resolvable pattern of fluorescent diI-LDL spots on the slide. The average was over 1–3 s of video frames. A background image was taken of a slide containing only PBS, and was subtracted from the diI-LDL image. The image was normalized with the fluorescence image from a film of uniformly distributed diI in Formvar plastic (manufactured as described in Schneider and Webb, 1981) to correct for varying illumination and gain over the image's spatial extent.

We obtained the distribution of fluorescence powers from diI-LDL on this microscope slide, and determined n, the mean number of diI molecules in single diI-LDL, as in Gross and Webb (1986, 1988) and Ghosh (1991). Based on this, we were able to determine how many unresolved diI-LDLs were clustered within each imaged fluorescent spot.

Any noise in the system, spatial variations of intensities, or any uncertainties introduced during background subtraction, will broaden the fluorescence power distribution. A particle in close proximity to another will have an extra power contribution added to its own power due to the two images overlapping. This will also cause the fluorescence power distribution to broaden. These factors all affect the goodness of the Poisson fit. Thus, this method leads to lower estimates for n than its actual value. To ensure we are in the right range and to ascertain that we are detecting single diI-LDL molecules, we turn to the other methods to provide independent determinations of n. However, this does not significantly change the classification of receptors into their cluster sizes, which is based on where their power lies within the distribution (Ghosh, 1991).

Spectrophotometry

To determine n spectrophotometrically, we compared absorbances of known concentrations of diI and diI-LDL in a solvent. The absorbance spectra of diI in DMSO or ethanol, and of diI-LDL in saline, has a double-peaked curve with the minor peak at 524 nm and the major peak at 554 nm. We measured the absorbance at these two wavelengths, as well as at 546 nm, the excitation wavelength in our microscope experiments. We measured the molar extinction coefficient, ϵ, for diI in DMSO and ethanol to be 7.4×10^4 M^{-1} cm^{-1} and 10.4×10^4 M^{-1} cm^{-1}, respectively. Our values for diI in ethanol differ slightly from the values listed in the Molecular Probes catalogue, and from those published by Sims et al. (1974). However, this should have only a minor effect on the final determination of n.

Absorbances were also taken of diI-LDL dissolved in the same solvent used for diI. This was to ensure that the diI associated with LDL, now surrounded by solvent, would have the same extinction coefficient as the diI in solvent measured earlier. From the absorbance and the concentration of LDL, we obtain n, the number of diI molecules in each diI-LDL (Ghosh, 1991).

A limitation of this method occurs if the diI-LDL sample contains extra diI not associated with LDL. This would result in a higher value of n than would be seen by other methods. The results of this absorbance method, and comparisons with the other two methods, are shown in Table 2.

Micro-spectrofluorometry

We next confirmed n by micro-spectrofluorometry. This was done by first measuring the fluorescence power to be detected from a single diI molecule with our camera. We then spread diI-LDL particles on a microscope slide and measured the fluorescence power of those diI-LDLs we believed to be monomers. These were the particles whose powers fell in the first peak of the fluorescence power distribution. The fluorescence power of diI-LDL was divided by the power per diI to obtain n.

To measure the fluorescence power collected per diI molecule, we made an optically thin film of diI dissolved in DMSO. Absorbance (a_{546}) of the diI-DMSO solution, for a 1 cm-pathlength at 546 nm, was around 0.03. We put a small drop of this diI-DMSO solution (~2 μl) on a microscope slide. Placing a 22 × 22 mm number 1 coverslip on top of the drop, we squeezed gently until the liquid spread evenly out, and then sealed the edges. We placed the diI-DMSO thin film on the microscope, excited at 546 nm, and recorded its fluorescence power with the camera.

Dividing the fluorescence power of diI-LDL by that of diI, gives the following expression for n

$$n = \frac{P_L N_0 A d a_{546}}{P_D \epsilon_L l Q}. \tag{9}$$

For each newly made batch of diI-LDL, we measured its power, P_L, and the power from a freshly made thin film of diI in DMSO, P_D. The other parameters we measure to apply Eq. 9 and thus determine n, were: d, the diI-DMSO film thickness; A, the area of one pixel; a_{546}, the 546-nm absorbance of the diI-DMSO film for a $l = 1$ cm pathlength; ϵ_L, the extinction coefficient of diI-LDL in PBS; and Q, the ratio of the quantum yields of diI in LDL in PBS with that of diI in DMSO.

The same diI-LDL image used for multiple Poisson fitting, was also used to obtain the power of single diI-LDLs. This was measured in ADU, and was the value at the peak of the monomeric diI-LDL distribution (1st peak). The error was the width of the distribution.

The diI-LDL extinction coefficient, ϵ_L, was obtained in PBS, and was the same as the diI-LDL extinction coefficient in DMSO within experimental error.

Image acquisition on a diI-LDL sample and a diI-DMSO thin film are done one after the other to ensure the same illumination and imaging conditions. The illumination power at the back focal plane of the objective was measured by a photodiode placed at the back aperture of a hollowed objective shell. The power was typically in the range of 1.5 mW.

Before use, the diI-DMSO film's image was averaged for the same amount of time and background-subtracted as was done for the diI-LDL image. We select a large region of the image and histogram the pixel powers to get the mean power per pixel, P_D. Thus, the area A used in Eq. 9 is the area of one pixel. The absorbance, a_{546}, of the diI-DMSO solution that was used to make the film, was around 0.03. This low value ensured an optically thin specimen with no artifacts from any inner filter effects.

To measure the thickness, d, of the thin film, we used a Biorad MRC600 laser scanning confocal microscope (Biorad, Cambridge, MA). X-Z images were taken on various parts of the film, and the separate measurements were averaged to determine its thickness. The dilute sample gave a weak signal, so we averaged the signal to improve image contrast, and thus, to better determine the sample thickness. A typical measurement would step 0.2 μm in the z direction. The typical range of film thicknesses would be 3–5 μm. This measured film thickness differs from the actual thickness due to a longitudinal magnification factor. This factor is proportional to the ratio of the indices of refraction of DMSO and immersion oil, and is known as the Maxwell elongation formula (Born and Wolf, 1959). The Zeiss immersion oil we used has an index of refraction of 1.518, and DMSO's index of refraction is 1.479, so the factor to mutiply the measured thickness, in order to get the actual thickness, is 0.974.

The quantum yields of diI in LDL and diI in DMSO are not the same. To measure Q, identical amounts of diI-LDL were diluted in PBS and in DMSO. Assuming DMSO fully dissolves diI-LDL, this meant we had the same amount of diI in DMSO as we had in LDL. Fluorescence emission spectra of these samples were obtained using a spectrofluorometer, with excitation at 546 nm with a resolution of 8 nm, and the emission stepped from 560 to 698 nm at 1-nm intervals with 4-nm resolution. For concentrations of diI-LDL above 0.5 μg/ml, the ratio of the fluorescence of diI in LDL in PBS to diI in DMSO was $Q = 0.7$ (Ghosh, 1991).

The measured parameters for five different combinations of different diI-LDL and diI-DMSO thin film batches are shown in Table 1. The first three batches used the video camera-intensifier system. The last two batches used the CCD camera as a detector. The values for n, obtained by using these parameters in Eq. 9, are shown in Table 2.

Number of photons (shot-noise calibration)

We also determine n micro-spectrofluorometrically by dividing the number of photons per unit time from single diI-LDLs on a slide, by the number of photons per unit time from diI in the diI-DMSO thin film. The pixel intensities are proportional to the number of photons detected per unit time, and this number of photons was determined by analyzing the shot noise limited signal as described earlier.

To determine n, we recorded a sequence of 150 images of a diI-DMSO film, and of diI-LDL on a coverslip as described earlier. We also recorded images from a slide of PBS in the same manner, to measure the number of background photons, not associated with the sample. We used the same thin film of diI in DMSO and same batch of diI-LDL as in batch 1 in Tables 1 and 2. The number of diI molecules per pixel in the diI-DMSO thin film image is

$$N = \frac{a_{546} A d N_0}{10^3 \epsilon l}, \tag{10}$$

TABLE 1 Measured values of parameters used to get n by microspectrofluorometry, for different diI-LDL and diI-DMSO thin film batches

Batch	P_L (ADU)	ϵ_L (cm^2/mol) $\times 10^9$	$\langle P_D \rangle$ (ADU)	A (cm^2) $\times 10^{-10}$	d (cm) $\times 10^{-4}$	a_{546} $\times 10^{-2}$
1	106 ± 26	2.74 ± .03	8.4 ± 2.9	4.0 ± .2	3.88 ± .56	3.69 ± .03
2	93 ± 16	.993 ± .002	13.3 ± 2.8	4.0 ± .2	4.84 ± .43	3.80 ± .03
3	69 ± 15	.86 ± .17	13.3 ± 2.8	4.0 ± .2	4.84 ± .43	3.80 ± .03
4	139 ± 31	1.95 ± .02	22.8 ± 1.5	2.4 ± .2	5.30 ± .71	6.10 ± .01
5	139 ± 31	1.95 ± .02	9.3 ± 1.0	2.4 ± .2	3.77 ± .41	2.06 ± .01

P_L is the diI-LDL power, and $\langle P_D \rangle$ is the mean power per pixel from the diI-DMSO thin film. A is the area of one pixel, and d is the diI-DMSO thin film thickness. The diI-LDL extinction coefficient is given by ϵ_L, and the 546-nm absorbance of the diI-DMSO solution in the thin film, for a 1-cm pathlength, is a_{546}.

TABLE 2 Values of *n*, the number of dil molecules per LDL particle, obtained for different batches, by the three different methods

Batch	Poisson Fit	Absorbance	DiI-DMSO Film	Shot Noise
1	19	31	23	33
2	45	23	45	—
3	28	26	38	—
4	20	25	21	—
5	20	25	13	—

Shot noise analysis was done only on batch 1, and absorbance using ethanol instead of DMSO as a solvent gave $n = 31$ (batch 2) and $n = 24$ (batch 3).

where ϵ is the molar extinction coefficient for dil in DMSO at 546 nm, a_{546} is the thin film absorbance, l is 1 cm, d is the thin film thickness, A is the area of 1 pixel and N_0 is Avogadro's number. For the sample we used, we got 46.7 dil fluorophores per pixel.

Using Eq. 6, we determined the number of photons from single pixels of the dil-DMSO sample, and the number of photons from the same single pixel of the PBS sample. Subtracting these two, we determined that the net number of photons detectable above noise, from a single pixel containing a mean of 46.7 dil molecules, to be 36.7 ± 13.4. Dividing by the number of dils per pixel, we can determine the mean net number of photons from a single dil molecule.

The individual pixels we used to determine the number of photons detected in the dil-DMSO film images were the same pixels as covered by the single imaged dil-LDLs. This was done to minimize any geometric variability arising from different spatial locations on the screen. We first determined which dil-LDL particles to examine by choosing those that appeared as singles within one SD, from the multiple Poisson fitting technique. We counted 81 of the dil-LDL spots in the field we imaged as singles. The gross number of photons was determined by using Eq. 6 over the area covered by each dil-LDL. The background photons were determined for the same area by applying the same relation on the PBS images. The net number of photons detected above noise from a single dil-LDL was obtained by subtracting these two quantities, and was 33.5 ± 17.3.

To determine n, we divided the net number of photons from each single dil-LDL in PBS by the net number of photons from single dil molecules in DMSO imaged from the same area, and then multiplied this by Q, the ratio of quantum yields of dil in LDL in PBS and dil in DMSO ($Q \sim 0.7$). Taking the mean over the 81 single dil-LDLs, we get $n = 32.6 \pm 18.3$, which compares favorably with n obtained by other methods for the same batch of dil-LDL (Table 2).

Using Eq. 5, we can determine the smallest number of dil molecules detectable by our system, where we used 150 images, each of which was the average of 32 frames with exposure times of 33 ms per frame. With 46.7 dil fluorophores per pixel in DMSO, we get a mean of 36.7 photons per pixel. Taking the square root, we get a signal-to-noise ratio of 6.06 (Eq. 5). To be able to detect 1 photon per pixel above noise means that a signal-to-noise ratio of at least 1 is needed. A signal-to-noise of 1 is obtained from 7.7 dil molecules per pixel. Thus, with our system, the smallest number of dil molecules per pixel in DMSO we can detect above noise is 7.7. The number of dils detectable in a saline and lipid environment, such as that encountered in the LDL coat, is larger, due to dil's higher quantum yield in DMSO. To detect a single dil molecule, enough photons would have to be collected so that the signal-to-noise from a single dil molecule was greater than 1. Because the signal-to-noise is proportional to the square-root of the number of detected photons, increasing the detection time by a factor of 60 (7.7 squared) should allow enough photons to be collected in order to detect a single dil molecule with our system, assuming minimum photobleaching during this time. Additionally, increasing the excitation intensity would allow an increase in the number of detected photons, but this also carries the risk of increased photobleaching.

Results: comparisons between the three methods for different dil-LDL batches

Table 2 lists five examples of n, obtained from Poisson fitting, spectrophotometry, and thin-film microspectrofluorometry. These are from four different batches of dil-LDL, and case 4 and 5 are the same dil-LDL batch, but different dil-DMSO thin film specimens. The n listed under Poisson fitting was the value obtained from the best fit to the distribution (Gross and Webb, 1986; Ghosh, 1991). This was done for the first three batches, which were obtained by the video camera-intensifier system where the photon to ADU conversion had been determined. The values for n are all within a factor of 2 of each other, indicating that we are able to measure and confirm n by these three independent methods.

We also measure n spectrophotometrically for batches 2 and 3 using ethanol, instead of DMSO, as a solvent. This gave $n = 31$ for batch 2, and $n = 24$ for batch 3. The shot-noise analysis to determine n from the number of photons, was carried out on batch 1. This gave $n = 32.6$.

We believe that the particles we identify in images as monomeric dil-LDL, are indeed monomeric dil-LDL, as seen by the similar values of n obtained by the different methods. If we were not able to detect single dil-LDL particles, and were instead detecting some larger dil-LDL aggregation state, then the values of n obtained by the different methods would differ by more than a factor of two. More specifically, if we were imaging clustered dil-LDLs instead of single dil-LDLs, then n obtained by absorbance would be a factor of two or more lower than n determined by the imaging techniques. We see in Table 2 that n obtained by absorbance matches the n values obtained by the other methods within a factor of 2, thus providing further support to our ability to detect single dil-LDLs. In addition, if we were identifying clustered dil-LDLs as individuals, the binned fluorescence powers would show peaks of distinct cluster sizes between the two peaks we identify as the monomeric and dimeric peaks. We do not observe this, and instead find that the powers of the different

cluster size peaks we detect are integer multiples of the power of the first peak, which we identify as containing monomers.

Detection and tracking of individual and clustered LDL-R molecules on the cell surface

We have shown that we detect single diI-LDLs. In addition, we can determine the aggregation size of larger clusters of diI-LDL. This enables us to track single and clustered LDL-R molecules, and thus, examine their mobility as a function of their aggregation size. We will now illustrate the capabilities of the techniques we have developed. The analysis of and conclusions from using these methods to studying LDL-R dynamics and aggregation on cell surfaces is presented elsewhere (Ghosh and Webb, 1989, 1990, in preparation; Ghosh, 1991; Slattery et al., 1991; Brust-Mascher et al., 1992, 1993).

A fluorescence image of a JD fibroblast labeled with diI-LDL is shown in Fig. 6. The white spots in this image are the diI-LDL-labeled receptors. The brighter spots are large clusters and contain a larger number of unresolved diI-LDLs than the dimmer spots. 150 time-lapse fluorescent images were taken of this cell at a rate of an image every 1.6 s. The trajectories of the LDL-Rs on this cell obtained from automatic tracking, are shown in Fig. 7. The time evolution of the

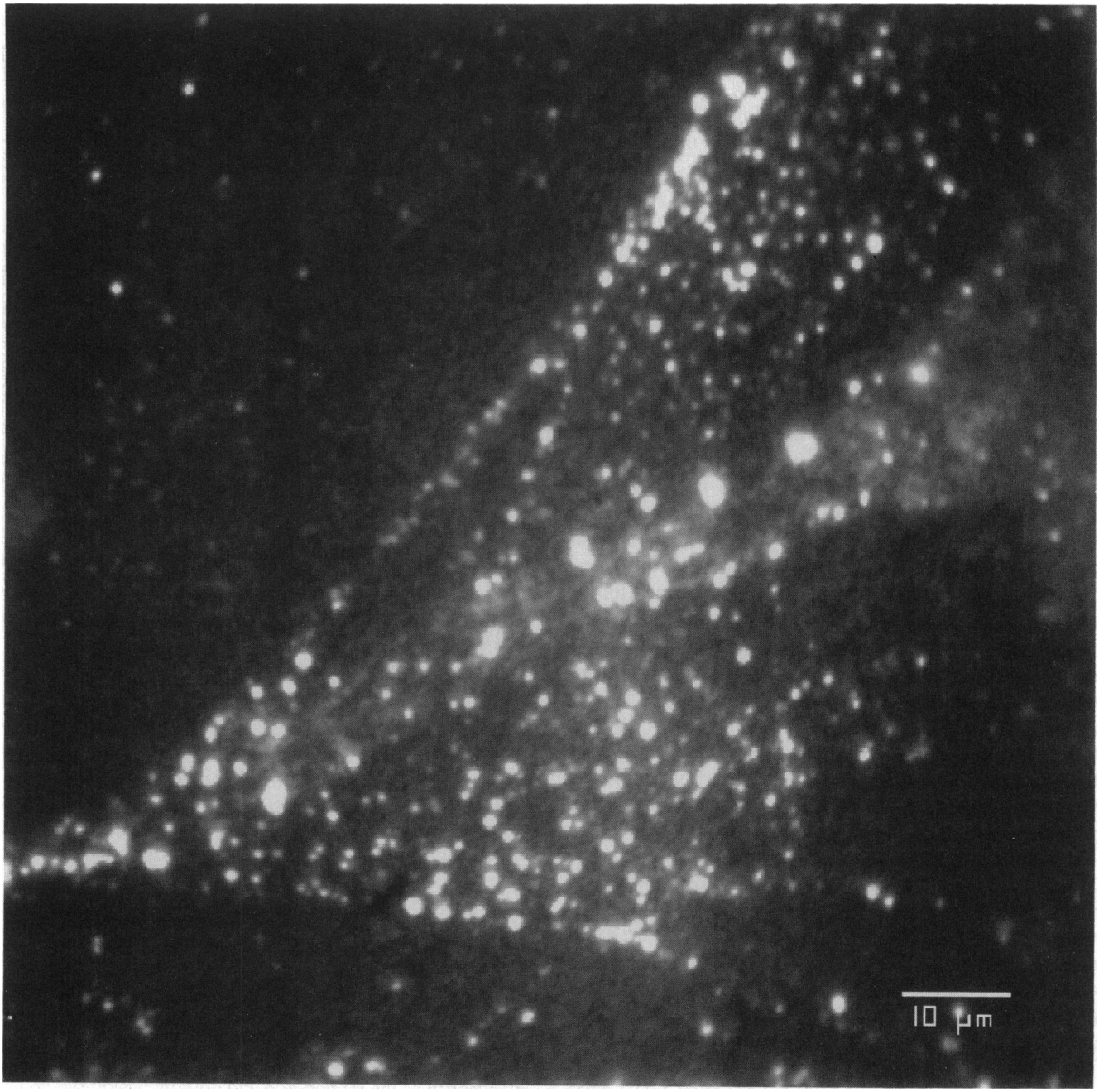

FIGURE 6 Fluorescent image of a JD fibroblast whose LDL-Rs are labeled with diI-LDL. Scale bar = 10 μm.

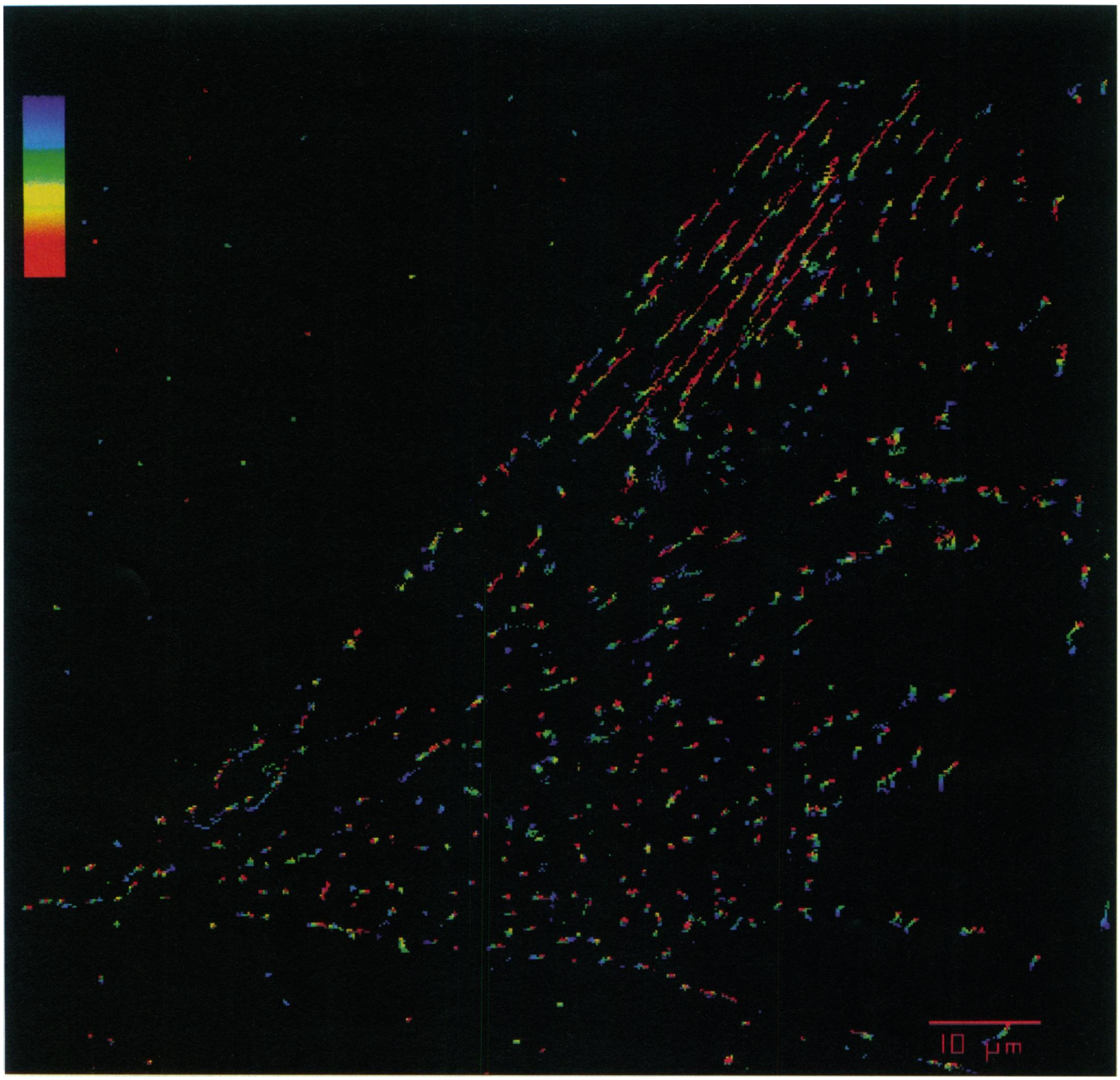

FIGURE 7 Trajectory map of the cell from the previous figure showing the tracked movements of the labeled cell surface LDL-Rs on the JD fibroblast through a sequence of 150 images, 1.6 s apart. Pseudo-color denotes the temporal evolution of the tracks, starting from dark blue at the positions in the first image, and progressing to red, at the end of the experiment, 4 min later. Scale bar = 10 μm.

trajectories is shown in pseudo-color, where the particles' positions in the first image is in dark blue, and evolves up the color spectrum to red for the final image, 4 min later. In this manner, not only can one see where a particle moved, but also when it moved there, and, thus, see the vector fields and global patterns of motion of LDL-Rs on the cell. Each particle's position at every time point is known with a precision of 30 nm. However, Fig. 7 is a low resolution map of all the particles' trajectories on the cell, and the scale bar is 10 μm. The concerted, directed motion of many LDL-Rs near the top of this image is easily seen in this low resolution map, but there are many more interesting movements of particles that become apparent in higher resolution maps where the high precision localization of the particles' is taken advantage of, as shown in Figs. 9 and 10.

The number of unresolved LDL-Rs each fluorescent spot contained was obtained from multiple-Poisson fitting, and is shown in the pseudo-color map in Fig. 8. The number of dil fluorophores per LDL for this batch of dil-LDL was obtained from multi-Poisson fitting to be 24. Each color represents a separate cluster size, and if a particle's power was between the power range of two sizes, it was depicted by a spot show-

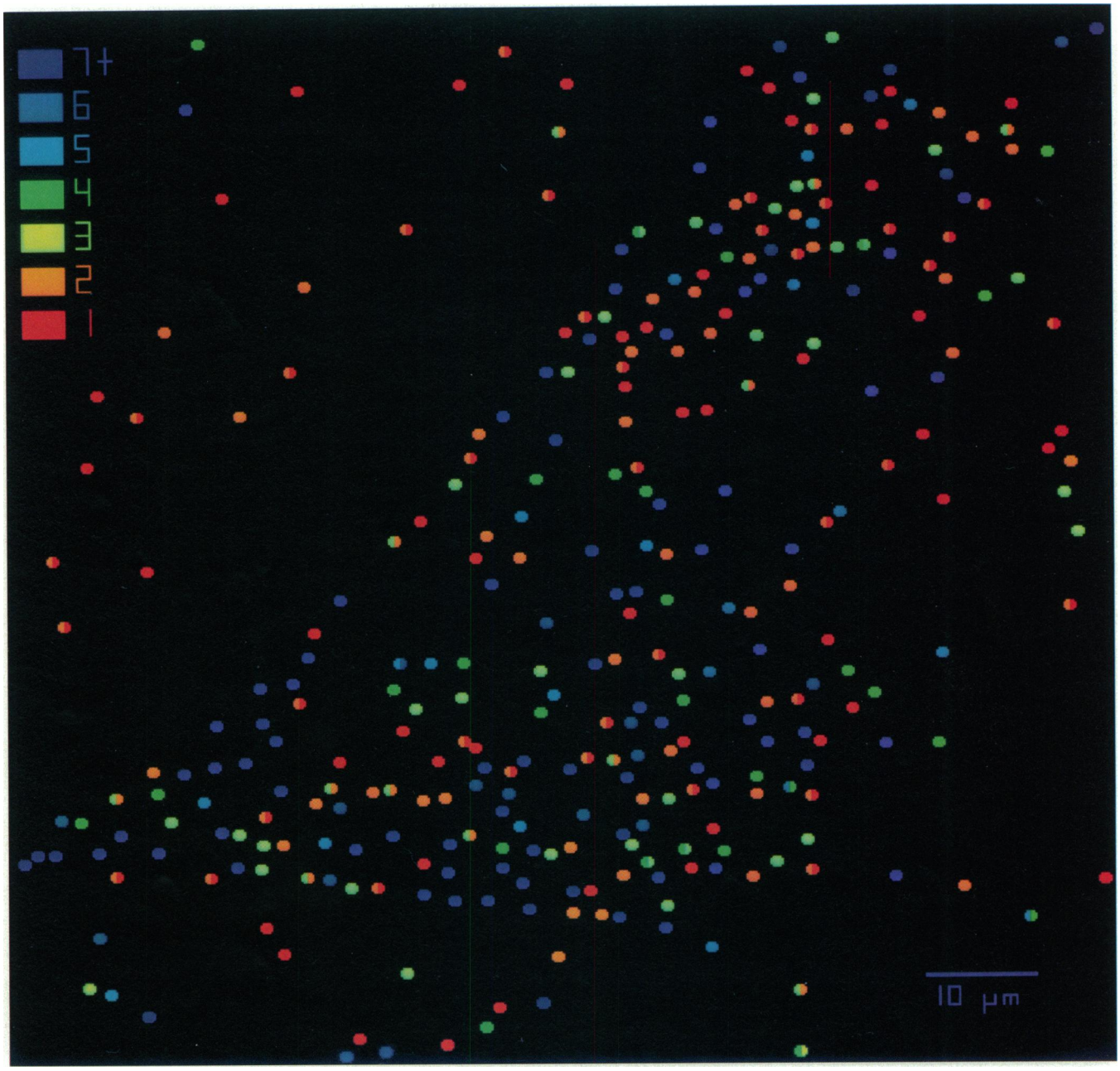

FIGURE 8 Map of the size of LDL-R clusters on the JD cell shown in the previous figure. Pseudo-color represents the separate aggregation states. If the number of LDL-Rs in a spot is intermediate between two cluster sizes, it is depicted by a spot with both colors. Cluster sizes from 1 to 6 were resolved, and represented by separate colors. Larger clusters were represented by the same color.

ing the colors of both sizes. A maximum resolvable cluster size of 6 implies 26 dil fluorophores in a single dil-LDL. This was an upper bound for the number of dil molecules in a single LDL, for this batch of dil-LDL. All clusters containing seven or more unresolved LDL-Rs are shown by the same color in Fig. 8.

Examples of trajectories of clustered receptors tracked with 30-nm precision and comparisons with immobile particle (slide attached) tracks are shown in Figs. 9 and 10. As can be seen, a whole host of interesting motions can be seen at this precision, and the (slide attached) immobile particle's drift is dwarfed by the scale of LDL-R movement. In both of these figures, the pixel size was set at 30 nm when plotting the trajectories. This was to indicate the scale of our precision in determining a particle's position relative to the overall particle motion. Fig. 9 shows three receptor clusters undergoing anomalous diffusion, with the lower two particles showing some correlation. In a low precision map (such as in Fig. 7), these three particles would appear to be acting in concert in a directed manner, and the details of their motion would not be evident as in Fig. 9. In contrast, the particle in Fig. 10 is undergoing directed motion with constant velocity, as seen in this high precision trajectory map. A more complete description and analysis of the different types of motion

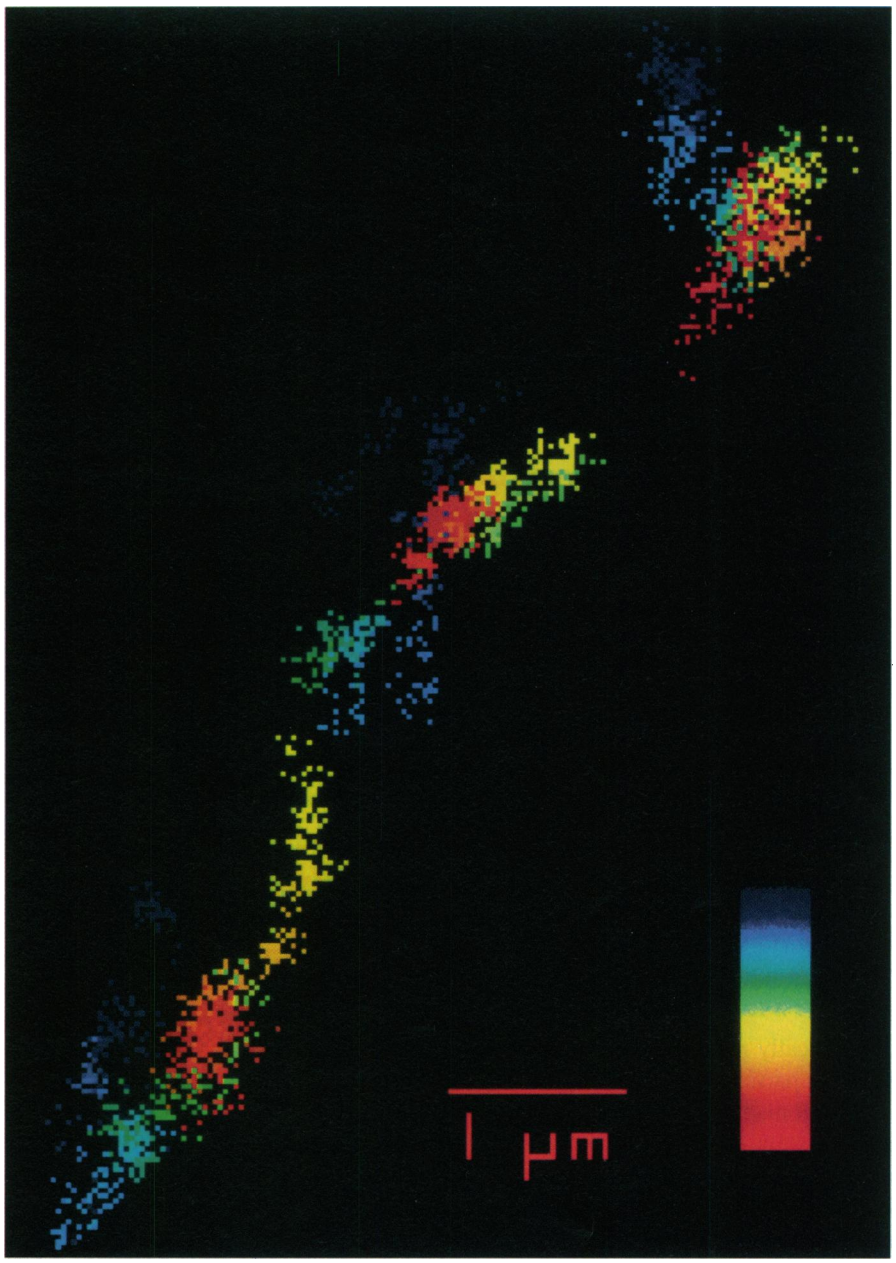

FIGURE 9 High-precision trajectories for three particles close to each other on the cell surface, undergoing anomalous diffusion. Each pixel in this plot is set at a size of 30 nm to represent the limit in localizing a particle. Pseudo-color represents time evolution of this particle through the 900 images, 0.3 s apart, giving a total time of 5 min. The lower two particles show some correlation in their movement, as seen from the general directions of their motions. This high precision trajectory map reveals the complexity of each particle's motion and the slight correlation they have with each other, whereas in a low precision map, such as in Fig. 7, these particles would appear to have directed motion, and move in concert with each other. Scale bar = 1 μm.

undergone by LDL-Rs on cell surfaces and their relation with their clustering states is given elsewhere (Ghosh and Webb, in preparation).

DISCUSSION

We have described the development of a powerful and sensitive tool to study the mobilities of individual cell surface receptor molecules. Among the capabilities we have developed is the ability to track automatically large numbers of individual and clustered LDL-R molecules simultaneously on the cell surface with high precision and without the need for user intervention. The importance of automatic tracking is that a large number of particles can be easily tracked, thus reducing the statistical variations between trajectories and making trends in cell surface particle motions more evident. This point is implicit in the probability density distributions and other statistics used by Saxton in his computer simulations of particles moving on the cell surface (Saxton, 1993). The bright fluorescent ligand, diI-LDL, is used to label individual LDL-R molecules, and to resolve successfully and track the motions of individual and clusters of LDL-Rs, the density of fluorescent spots should be substantially less than 1 per μm^2.

We have described four different methods of ascertaining that we can detect individual diI-LDLs. Using the brightness of each imaged fluorescent spot, we show how to determine the number of unresolved individual diI-LDLs within the spot. This method can be used to assess the aggregation state of individual LDL-R molecules on the surface of cells. The resolution of the different number of LDL-Rs in a spot is limited by the mean number of diI fluorophores per LDL. We

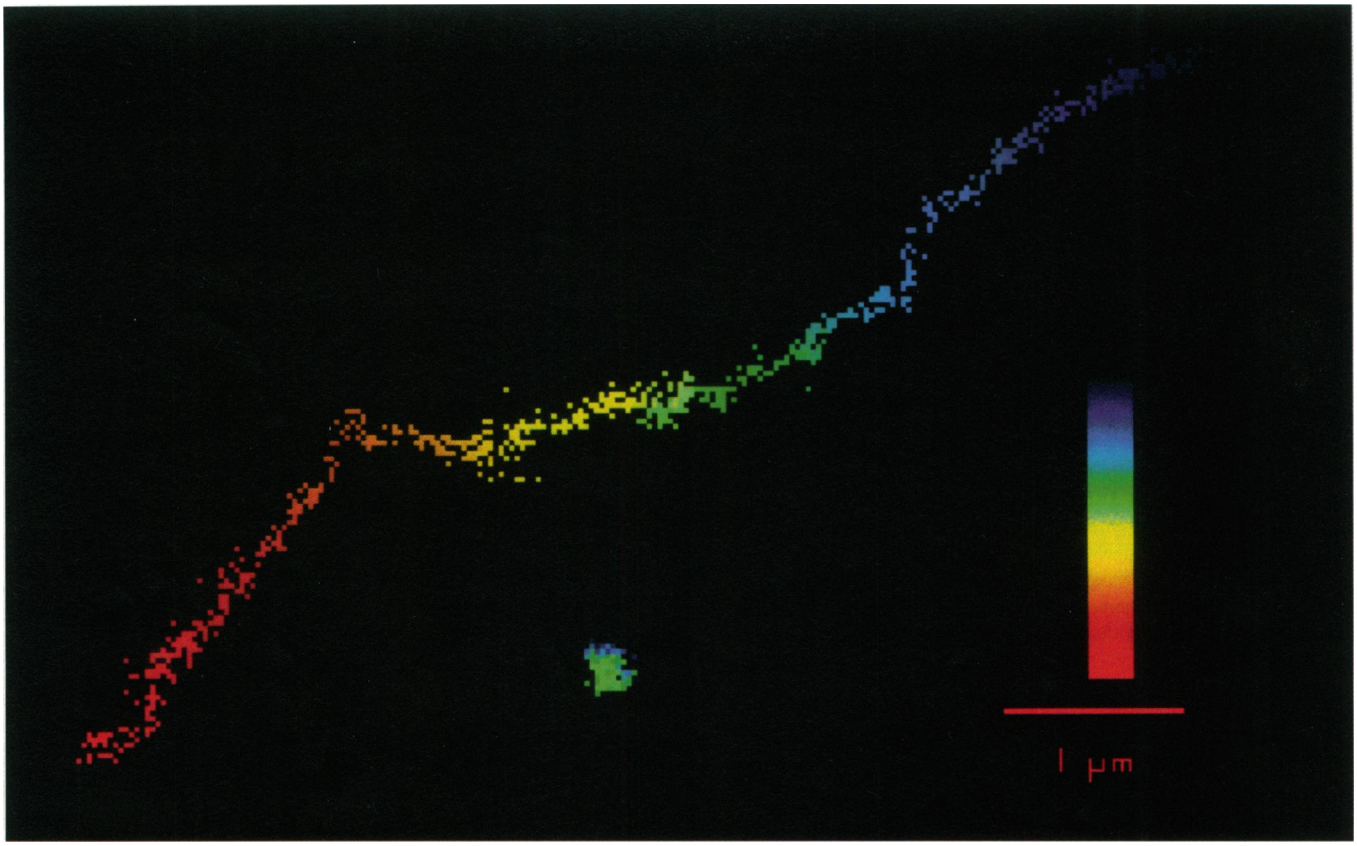

FIGURE 10 High precision map of a particle exhibiting directed motion with constant velocity. The particle was tracked through 900 images acquired at a rate of 3 images/s, giving a total time of 5 min. Pseudo-color represents the temporal evolution of the trajectory. The scale used in drawing this plot is such that each pixel is set at a size of 30 nm to represent the limit in localizing a particle, and represents a separate time point. An immobile particle's trajectory is shown for comparison. The scale bar is 1 μm.

can typically resolve up to a cluster containing 5 dil-LDLs. Brighter particles increase the size to which we can resolve.

Spatial mapping of particles and displaying their temporal evolution by color immediately yields phenomena not directly observable by FPR. One can simultaneously see the spatial and temporal evolution of the particles over the whole cell, whereas in FPR one was restricted to a small spot or a periodic pattern. The map of particle trajectories in Fig. 7 shows that some LDL-Rs move in a nonrandom, albeit independent, directed manner (near top of image). There also seems sometimes to be a strong correlation between the directed motions of neighboring particles on this immobile cell. There also exists areas on the same cell's surface where the LDL-R's mobility behaves in a different manner from the striking directed motion near the top of the image. This global picture of movement of LDL-Rs indicates a degree of cell membrane heterogeneity. The high precision trajectory maps of Figs. 9 and 10 reveal details of LDL-R motion not easily apparent in the low resolution maps such as that shown in Fig. 7.

The signal of our video camera-intensifier system is shot-noise-limited. We have shown by computer simulation that for a noise- and resolution-limited system the precision in localizing and tracking a particle should be proportional to the reciprocal of the signal-to-noise. Decreasing the magnification onto the camera faceplate does not alter the precision because the higher signal-to-noise per pixel is offset by the smaller number of pixels covered by the particle. Experimentally we find that there is a barrier to improving precision with higher signal-to-noise, and at a signal-to-noise of greater than 20 the tracking precision remains constant at about 15 nm in our system. This is due to the slow drift of the system, which was the dominant contribution to particle localization sensitivity at high signal-to-noise. DiI-LDL provides a signal-to-noise around 6, which was obtained with our rather dim illumination from images where each image was the average of 32 frames with an exposure time of 33 ms per frame. At this level the main noise contribution is from the shot-noise-dependent measurement uncertainty, giving a localization precision of 30 nm. This implies that there is no basic barrier to high precision provided that more light is collected (higher signal-to-noise), such as from brighter particles and stronger illumination, and the mechanical noise of the system is reduced. Thus, precisions approaching 1 nm should be attainable. Note that the cells were immobile, and evidence of cell stability is manifest in the concerted motion of LDL-Rs with its neighbors in Fig. 7.

Note that the excitation illumination we used was sufficiently dim so that 5 min of continuous illumination produced less than 10% photobleaching of fluorescence. The

excitation intensity can be increased by a couple of orders of magnitude, and the fluorophore would still not saturate. This would allow the image aquisition time to be reduced by a similar factor for equivalent negligible photobleaching for the same number of images.

Denk and co-workers (Denk et al., 1986, 1989; Denk, 1989; Denk and Webb, 1990) showed that they could measure motion displacements with high sensitivity (10^{-12} m $/\sqrt{Hz}$) over a wide bandwidth (1 Hz-100 kHz) using a differential micro-interferometer. Gelles et al. (1988) used differential interference contrast (DIC) microscopy to observe 190 nm diameter plastic beads immobilized on a glass microscope slide. They were able to localize these beads with a precision of 1–2 nm. These two cases of better precisions are probably due to the higher signal-to-noise achieved by using DIC instead of fluorescence microscopy, and lower mechanical noise in their systems. For a shot-noise-limited instrument, the signal in DIC can be increased by the illumination intensity, whereas increasing the illumination intensity in fluorescence microscopy does carry the additional hazard of rapid photobleaching of the fluorophore. Kusumi et al. (1993) used the same technique as Gelles et al. (1988) and obtained a nominal diffusion coefficient for an immobile particle of 3.2×10^{-13} cm^2/s, a value comparable to the stationary particle diffusion coefficient we measured of 5.3×10^{-13} cm^2/s. This implies a similar level of drift, and the uncertainty in localizing a particle due to drift grows with the time interval between measurements (i.e., a 1.6 s time interval has a larger displacement than two images taken at video rates).

Geerts et al. (1987) have also described an automated tracking routine, where they image 40 nm colloidal gold to study cytoplasmic diffusion and kinesin influenced motion on microtubules. Although the gold particles are sub-resolution in size, they are strong scatterers of light and appear as black dots with high contrast in the images after video enhancement. They do not track the particles with high precision. However, this kind of marker could easily be implemented on their system. Quantitating the amount of scattered light would also indicate the aggregation state of their probe.

Both the fluorescent techniques we describe, and the bright light techniques of Gelles et al. and Geerts et al. have advantages. The high number of photons obtained from the bright light techniques implies a high signal-to-noise, which in turn implies a better precision in tracking than what we achieve in fluorescence. However, fluorescence microscopy provides an unambiguous identification of the particle being tracked. This can be a problem in DIC microscopy, where organelles and other cellular detritus may look similar to the probe. Pure brightfield microscopy resolves this problem somewhat because organelles appear almost transparent versus the strongly scattering gold probes.

Our fluorescent LDL is a biologically active indigenous ligand for its receptor, unlike colloidal gold and plastic beads. Also, fluorescence offers versatility by allowing the use of multi-color fluorescence microscopy where several separate cellular constituents labeled with different fluorophores can be observed simultaneously.

The techniques we have described can now be used to study the aggregation and mobility of individual and clusters of LDL-R molecules on the surface of cells, and results using these capabilities are presented elsewhere (Ghosh and Webb, 1989, 1990, in preparation; Ghosh, 1991; Slattery et al., 1991; Brust-Mascher et al., 1992, 1993). Studying the high precision motion of individual and clustered LDL-R molecules and the global patterns of all LDL-R movement over the cell surface provides a better insight into the restraints and controls to LDL-R motion than the ensemble-averaged diffusion coefficient and immobile fraction obtained from FPR experiments (Ghosh and Webb, 1989, 1990, in preparation; Ghosh, 1991; Slattery et al., 1991; Brust-Mascher et al., 1992, 1993). These methods can also be extended to carry out similar investigations on other receptor systems. We have modified diI-LDL to act as a monovalent ligand for the immunoglobulin E receptor, and have started investigating its mobility (Slattery et al., 1991). We have found similar types of motion for this system, as seen for the LDL-R. Thus, the automated detection and high precision tracking techniques we have developed can serve as a powerful and general tool in studying the mobility and clustering of individual receptor molecules on the surface of cells, and address questions regarding dynamic cellular control of receptors at the individual molecular level.

We are grateful to Drs. Michael Brown and Joseph Goldstein for their gift of the FH683 cell line and to Dr. Richard Anderson for his gift of anti-LDL-R antibodies, with which we checked expression of LDL-Rs on our cells. Eleanor Kable was invaluable with her help in making diI-LDL, growing and maintaining cell lines, and general biological advice. We also thank Ingrid Brust-Mascher, who helped in determining the limitations to high precision tracking and in the logistics of putting this paper together, Jan Speth, who assisted in the development of the automated tracking program, and Dr. Frederick Maxfield, who critically read this manuscript. Valuable discussions were also had with David Sandison, James Thomas, Toni Feder, and James Slattery.

This research was supported by the National Science Foundation (BBS 8714069 and DMB 8609084) and utilized facilities of the Developmental Resources for Biophysical Imaging and Optoelectronics (NIH-P41-RRO4224 and NSF-DIR8800278) and the Materials Research Center at Cornell University.

REFERENCES

Anderson, C. M., G. N. Georgiou, I. E. G. Morrison, G. V. W Stevenson, and R. J. Cherry. 1992. Tracking of cell surface receptors by fluorescent digital imaging microscopy using a charge-coupled device camera. *J. Cell Sci.* 101:415–425.

Axelrod, D., D. E. Koppel, J. Schlessinger, E. Elson, and W. W. Webb. 1976. Mobility measurement by analysis of fluorescence photobleaching recovery kinetics. *Biophys. J.* 16:1055–1069.

Axelrod, D. 1983. Lateral motion of membrane proteins and biological function. *J. Membr. Biol.* 75:1–10.

Barak, L. S., and W. W. Webb. 1981. Fluorescent low density lipoprotein for observation of dynamics of individual receptor complexes on cultured human fibroblasts. *J. Cell Biol.* 90:595–604.

Barak, L. S., and W. W. Webb. 1982. Diffusion of low density lipoprotein-receptor complex on human fibroblasts. *J. Cell Biol.* 95:846–852.

Bobroff, N. 1986. Position measurement with a resolution and noise-limited instrument. *Rev. Sci. Instr.* 57:1152–1157.

Born, M., and E. Wolf. 1959. Principles of Optics. Pergamon Press, (Sixth Edition, 1980).

Brown, M. S., and J. L. Goldstein. 1986. A Receptor-mediated pathway for cholesterol homeostasis. *Science.* 232:34–47.

Brust-Mascher, I., T. J. Feder, J. P. Slattery, B. Baird, and W. W. Webb. 1992. Constrained diffusion or immobile fraction on the cell surface: a new interpretation. *Mol. Biol. Cell* 3:306*a*. (Abstr.)

Brust-Mascher, I., T. J. Feder, J. P. Slattery, B. Baird, and W. W. Webb. 1993. FPR data on mobility of cell surface proteins reevaluated in terms of temporally constrained molecular motions *Biophys. J.* 64:354*a*. (Abstr.)

Cherry, R. J. 1979. Rotational lateral diffusion of membrane proteins. *Biochim. Biophys. Acta.* 559:289–327.

Denk, W., A. J. Hudspeth, and W. W. Webb. 1986. Optical measurement of the Brownian motion spectrum of hair bundles in the transducing hair cells of the frog auditory system. *Biophys. J.* 49:21*a*. (Abstr.)

Denk, W., W. W. Webb, and A. J. Hudspeth. 1989. The mechanical properties of sensory hair bundles are reflected in their Brownian motion measured with a laser differential interferometer. *Proc. Natl. Acad. Sci. USA.* 86:5371–5375.

Denk, W. 1989. Biophysical studies of mechano-electrical transduction in hair cells. PhD Thesis, Cornell University, Ithaca, NY.

Denk, W., and W. W. Webb. 1990. Optical measurement of picometer displacements of transparent microscopic objects. *Applied Optics.* 29: 2382–2391.

Geerts, H., M. De Brabander, R. Nuydens, S. Geuens, M. Moeremans, J. De May, and P. Hollenbeck. 1987. Nanovid tracking: a new automatic method for the study of mobility in living cells based on colloidal gold video microscopy. *Biophys. J.* 52:775–782.

Gelles, J., B. J. Schnapp, and M. P. Sheetz. 1988. Tracking kinesin-driven movements with nanometer-scale precision. *Nature.* 331:450–453.

Ghosh, R. N., D. Gross, and W. W. Webb. 1986. Effects of the calmodulin inhibitor stelazine on low density lipoprotein receptor motion on cell surfaces. *Biophys. J.* 49:356*a*. (Abstr.)

Ghosh, R. N., and W. W. Webb. 1987. Low density lipoprotein receptor dynamics on cell surfaces. *Biophys. J.* 51:520*a*. (Abstr.)

Ghosh, R. N., and W. W. Webb. 1988. Results of automated tracking of low density lipoprotein receptors on cell surfaces. *Biophys. J.* 53:352*a*. (Abstr.)

Ghosh, R. N., and W. W. Webb. 1989. Automated tracking of low density lipoprotein receptors on cell surfaces with nanometer precision. *Biophys. J.* 55:498*a*. (Abstr.)

Ghosh, R. N., and W. W. Webb. 1990. Evidence for intra-membranous constraints to cell surface low density lipoprotein receptor motion. *Biophys. J.* 57:286*a*. (Abstr.)

Ghosh, R. N. 1991. Mobility and clustering of individual low density lipoprotein receptor molecules on the surface of human skin fibroblasts. PhD Thesis, Cornell University, Ithaca, NY.

Goldstein, J. L., S. K. Basu, and M. S. Brown. 1983. Receptor-mediated endocytosis of low-density lipoprotein in cultured cells. *Methods Enzymol.* 98:241–260.

Gross, D., and W. W. Webb. 1986. Molecular counting of low-density lipoprotein particles as individuals small clusters on cell surfaces. *Biophys. J.* 49:901–911.

Gross, D. J., and W. W. Webb. 1988. Cell surface clustering mobility of the liganded LDL receptor measured by digital video fluorescence microscopy. *In* Spectroscopic Membrane Probes. L. Loew, editor. CRC Press, Boca Raton, FL. 19–45.

Innerarity, T. L., R. E. Pitas, and R. W. Mahley. 1980. Receptor binding of cholesterol-induced high density lipoproteins containing predominantly apoprotein E to cultured human fibroblasts with mutations at the low density lipoprotein locus. *Biochemistry.* 19:4359–4365.

Inoue, S. 1986. Video Microscopy. Plenum Press, New York.

Jacobson, K., E. Elson, D. Koppel, and W. W. Webb. 1982. Fluorescence photobleaching in cell biology. *Nature.* 295:283–284.

Kusumi, A., Y. Sako, and M. Yamamoto. 1993. Confined lateral diffusion of membrane receptors as studied by single particle tracking (nanovid microscopy). Effects of calcium-induced differentiation in cultured epithelial cells. *Biophys. J.* 65:2021–2040.

McCloskey, M., M. Poo. 1984. Protein diffusion in cell membranes: some biological implications. *Int. Rev. Cytol.* 87:19–81.

Peterson, G. L. 1977. A simplification of the protein assay method of Lowry *et. al.* Which is more generally applicable. *Anal. Biochem.* 83:346–356.

Pitas, R. E., T. L. Innerarity, K. S. Arnold, and R. W. Mahley. 1979. Rate equilibrium constants for binding of apo-E HDLc (a cholesterol-induced lipoprotein) low density lipoproteins to human fibroblasts: evidence for multiple receptor binding of apo-E HDLc. *Proc. Natl. Acad. Sci. USA.* 76:2311–2315.

Pitas, R. E., T. L. Innerarity, J. N. Weinstein, and R. W. Mahley. 1981. Acetoacetylated lipoproteins used to distinguish fibroblasts from macrophages in vitro by fluorescence microscopy. *Arteriosclerosis.* 1:177–185.

Ryan, T. A., P. J. Millard, and W. W. Webb. 1990. Imaging [Ca^{2+}] dynamics during signal transduction. *Cell Calcium.* 11:145–155.

Saffman, P. G., and M. Delbrück. 1975. Brownian motion in biological membranes. *Proc. Natl. Acad. Sci. USA.* 72:3111–3113.

Saffman, P. G. 1976. Brownian motion in thin sheets of viscous fluid. *J. Fluid Mechanics.* 73:593–602.

Saxton, M. J. 1993. Lateral diffusion in an archipelago: single-particle diffusion. *Biophys. J.* 64:1766–1780.

Schneider, M. B., and W. W. Webb. 1981. Measurement of submicron laser beam radii. *Appl. Opt.* 20:1382–1388.

Sims, P. J., A. S. Waggoner, C. H. Wang, and J. F. Hoffman. 1974. Studies on the mechanism by which cyanine dyes measure membrane potential in red blood cells phosphatidylcholine vesicles. *Biochemistry.* 13: 3315–3330.

Slattery, J. P., D. Holowka, R. N. Ghosh, W. W. Webb, and B. Baird. 1991. Bright fluorescent probe for high precision tracking of individual immunoglobulin E receptor molecules. *Biophys. J.* 59:384*a*. (Abstr.)

Thomas, J., and W. W. Webb. 1990. Fluorescence photobleaching recovery: a probe of membrane dynamics. Non-invasive techniques in cell biology. K Foskett, editor. Wiley-Liss Inc., New York. 129–152.

Webb, W. W., L. S. Barak, D. W. Tank, and E. S. Wu. 1982. Molecular mobility on the cell surface. *Biochem. Soc. Symp.* 46:191–205.

Webb, W. W., and D. Gross. 1986. Patterns of individual molecular motions deduced from fluorescent image analysis. applications of fluorescence in the biomedical sciences. Alan R Liss, New York. 405–422.

Yechiel, E., and M. Edidin. 1987. Micrometer-scale domains in fibroblast plasma membranes. *J. Cell Biol.* 105:755–760.